Insight in the Relationship between the Structure and Property of Methimazole Monolayers on a Silver Surface: Electrochemical and Raman Study

Rui Zhang, Ying Wen, Na Wang, Yao Wang, Yingying Wang, Zongrang Zhang, and Haifeng Yang*

Department of Chemistry, Shanghai Normal University, 100 Guilin Road, Shanghai 200234, P. R. China

Received: November 20, 2009; Revised Manuscript Received: December 25, 2009

Methimazole (MMI) monolayers on the silver surface were studied by electrochemical impedance spectroscopy (EIS), electrochemical polarization measurement, and surface-enhanced Raman scattering (SERS) spectroscopy. The EIS mechanism of the silver surface with MMI monolayers was fitted with the mode of *LR(QR)(QR)*, and the electrochemical polarization experimental results showed a high inhibitive efficiency around 82.6%. SERS results indicated that the MMI molecule with a tilted orientation anchored at the silver surface via S^6, N^2, and N^5 atoms, resulting in a strong interaction between the MMI molecule and the surface. In situ electrochemical SERS observation suggested that the molecule experienced a transition state of the adsorption because of the electrochemical hydrogen evolution reaction occurred about −0.1 V vs SCE.

1. Introduction

The methimazole (MMI) as an important antithyroid drug is widely used for the clinical treatment of hyperthyroidism.[1−3] Also, the MMI molecule is one of the azole derivatives that have widespread applications in the field of inhibition of metals from corrosion in some reports.[4,5] Herein, the anticorrosive feature of MMI as a potential inhibition reagent arouses our interest of observation. The MMI molecule possesses the thiol group and two nitrogen atoms. Nitrogen donates a lone pair of electrons to the thiocarbonyl group. Thus, the MMI molecule exists in two tautomeric forms, the thiol and the thione forms, which are shown in Scheme 1. The MMI in powder form has been characterized by Raman and infrared spectra as well as a detailed study in vibrations by quantum chemistry calculation.[6] The spectral result exhibits that the MMI mainly presents in the thione form.

Silver as a malleable and ductile noble metal is widely used due to its easy machining. However, it also suffers from tarnishing. For this reason, the silver protected by anticorrosion chemicals has been extensively investigated, for example, the azole and its derivatives of benzotriazole, 2-mercaptobenzothiazole, 3-amino-1,2,4-triazole, 2-amino-5-mercapto-1,3,4-thiadiazole, mercaptobenzoxazole, and 4-methyl-4*H*-1,2,4-triazole-3-thiol, etc.[7−15]

Observation of the coating on a metal surface for anticorrosion usually has been conducted by the transmission electron microscopy,[16] low energy electron diffraction,[17] UV photoelectron spectroscopy,[18] high-resolution electron energy loss spectroscopic,[19] and surface-enhanced Raman scattering (SERS) spectroscopic techniques. SERS spectroscopy is a very powerful tool of surface analysis because of its high sensitivity, surface specificity, and abundant molecular information along with no need for the strict condition of vacuum.[20−28]

Besides, electrochemical investigations for the anticorrosive films have been performed, especially by electrochemical impedance spectroscopy (EIS) and electrochemical polarization curve. EIS as a powerful, nondestructive, and accurate method has been successfully applied to the study of corrosion systems for 30 years for measuring corrosion rates.[29] At the same time, in order to access the charge transfer resistance or polarization resistance that is proportional to the corrosion rate at the monitored interface, EIS results are interpreted with the help of an equivalent circuit model of the interface. The polarization curve is generally used to estimate corrosion rate and other electrochemical parameters of the metals on the basis of Gauss−Newton nonlinear fitting.[30]

SCHEME 1: Molecular Structures of MMI in (a) Thione and (b) Thiol Forms

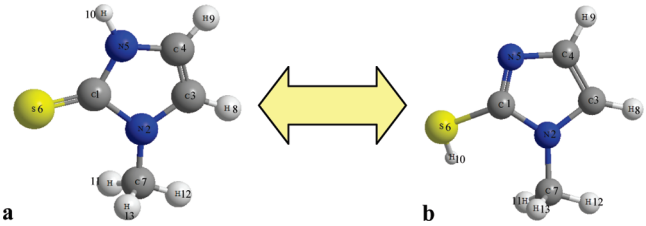

The aims of the present work are to examine the relationship between the anticorrosion behavior and the structure of the MMI coating on the silver surface via the self-assembled monolayer (SAM) technique with electrochemistry and SERS spectroscopy.

2. Experimental Section

2.1. Chemicals and Materials. Methimazole was purchased from Sigma-Aldrich Corporation. All reagents were of analytical grade, and all solutions were prepared with Milli-Q water.

A homemade three-electrode cell was used. The working electrode was made from a polycrystalline silver (99.99+%, Sigma-Aldrich) rod embedded in a Teflon sheath. The geometric surface area of Ag is ca. 0.025 cm^2. A platinum flake electrode and a saturated calomel electrode (SCE) were employed as the counter and reference electrodes, respectively.

2.2. Apparatus. A confocal Raman system (LabRam Π, Dilor, France) was used to record Raman spectra. The wavelength of the exciting radiation provided by an inner air-cooled He−Ne laser was 632.8 nm. A 50× long-working length

* To whom correspondence should be addressed. Phone/Fax: +86-21-6432-1648. E-mail: haifengyang@yahoo.com.

10.1021/jp911024d
Published on Web 01/29/2010

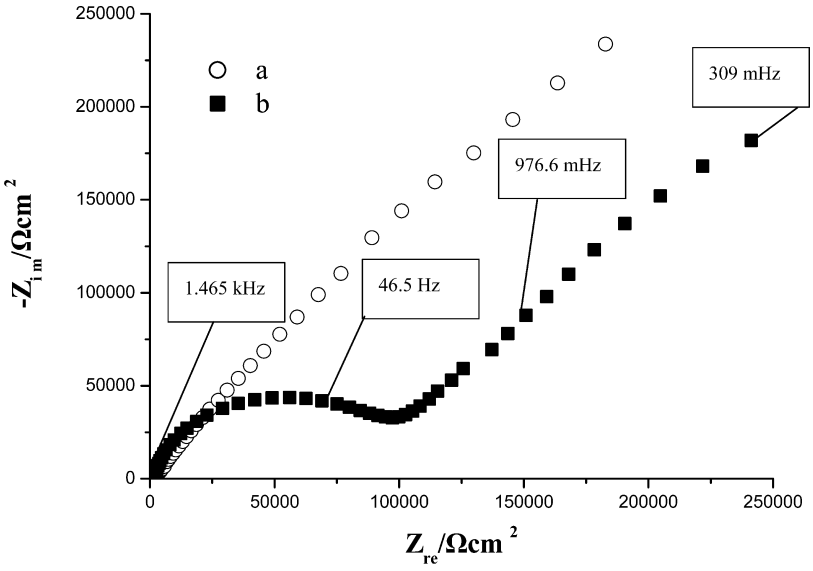

Figure 1. Nyquist impedance plots of (a) blank and (b) MMI monolayer modified silver electrode in 0.5 M KCl and 2.5 mM $[Fe(CN)_6]^{3-}$/$[Fe(CN)_6]^{4-}$ solution.

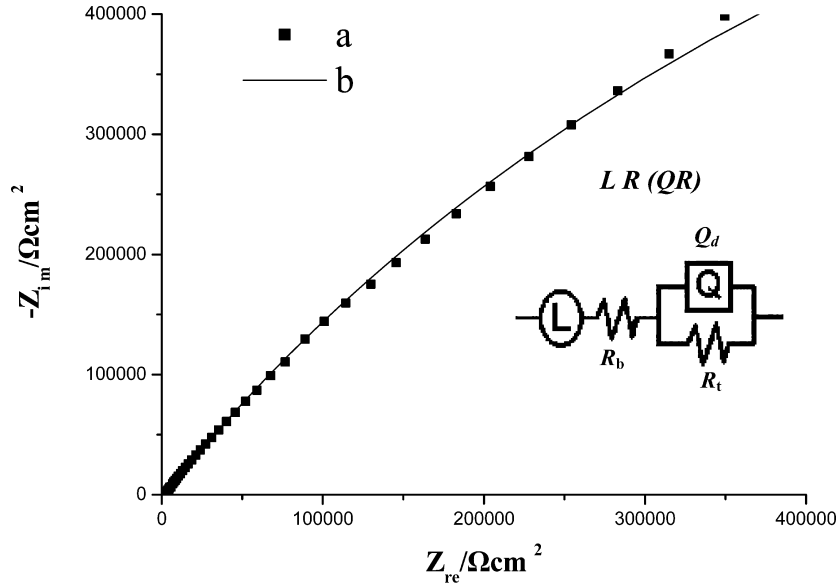

Figure 2. Nyquist impedance plots of a blank silver electrode in 0.5 M KCl and 2.5 mM $[Fe(CN)_6]^{3-}$/$[Fe(CN)_6]^{4-}$ solution: (a) experimental data and (b) curve fitting results.

objective was also used. The power and the size of the laser spot in diameter at the surface were 12 mW and 3 μm. The slit and pinhole were set at 100 and 1000 μm, respectively. Each spectrum was obtained using five accumulations, and the acquisition time in each case was typically 10 s. Calibration was done referring to the 519 cm^{-1} line of silicon.

The electrochemical measurements were conducted by a CHI660d electrochemistry workstation (Chenhua Instruments Inc.).

2.3. Details. ***2.3.1. Pretreatment for Electrode.*** Before the Raman scattering measurement, the silver electrode was sequentially polished with emery paper and 0.3 μm alumina/water slurries until a shiny, mirror-like surface was obtained, and then was ultrasonically washed with Milli-Q water. For SERS detection to obtain a necessary roughness of silver surface, the oxidation reduction cycle was performed[31] in a conventional three-electrode cell. All potentials cited in this paper have been converted to SCE.

2.3.2. Self-Assembled Monolayers (SAMs). To form the monolayers, the cleaned electrode was immersed into a solution containing 1×10^{-5} M MMI for 20 h at room temperature. The modified electrode was taken out of the solution and rinsed carefully with ethanol and Milli-Q water, and then dried prior to further investigation.

2.3.3. EIS Measurement. The EIS of silver electrodes with and without MMI monolayers were carried out in the 0.5 M KCl and 2.5 mM $[Fe(CN)_6]^{3-}$/$[Fe(CN)_6]^{4-}$ solution. A sinusoidal perturbation with 5 mV amplitude was applied at the formal potential, and the impedances were measured starting from open circuit potential in the frequency range from 0.01 Hz to 100 kHz. The impedance plots were fitted with a compatible electronic equivalent.

2.3.4. Polarization Measurement. Tafel curves of the silver electrodes with and without MMI monolayers were conducted in the 0.5 M KCl and 2.5 mM $[Fe(CN)_6]^{3-}$/$[Fe(CN)_6]^{4-}$ solution at room temperature. The scan rate was set at 10 mV/s.

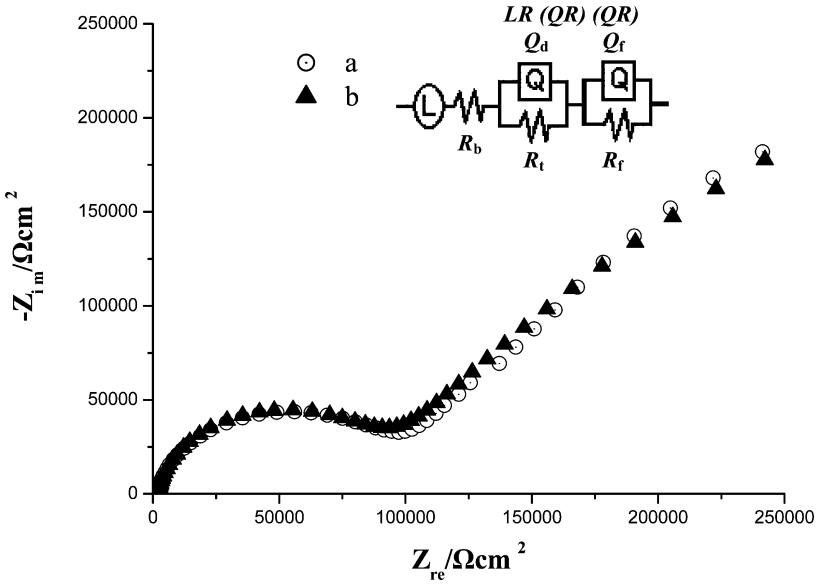

Figure 3. Nyquist impedance plots of MMI monolayers formed at a silver electrode in 0.5 M KCl and 2.5 mM $[Fe(CN)_6]^{3-}$/ $[Fe(CN)_6]^{4-}$ solution: (a) experimental data and (b) curve fitting result.

TABLE 1: Values of Electrochemical Parameters for a Blank Silver Surface Obtained by Fitting the Experimental Impedance Data Using the Suggested Equivalent

			Q_d		
solution	L/(Henry cm^2)	R_b/(Ω cm^2)	$Y_{film}{}^a$	n	R_t/(Ω cm^2)
0.5 M KCl and 2.5 M $[Fe(CN)_6]^{3-}$/$[Fe(CN)_6]^{4-}$	5.65×10^{-5}	1725	1.415×10^{-6}	0.662	2.219×10^{6}

[a] The dimensions are S; s^n cm^{-2}; if $n = 1$, they are F cm^{-2}.

TABLE 2: Values of Electrochemical Parameters for MMI Monolayers on the Silver Surface Obtained by Fitting the Experimental Impedance Data Using the Suggested Equivalent

			Q_{film}			Q_d		
solution	L/(Henry cm^2)	R_b/(Ω cm^2)	$Y_{film}{}^a$	n	R_{film}/(Ω cm^2)	$Y_{film}{}^a$	n	R_t/(Ω cm^2)
0.5 M KCl and 2.5 M $[Fe(CN)_6]^{3-}$/$[Fe(CN)_6]^{4-}$	1.949×10^{-21}	1727	3.816×10^{-8}	0.943	8.248×10^{4}	2.386×10^{-6}	0.652	1.12×10^{6}

[a] The dimensions are S; s^n cm^{-2}; if $n = 1$, they are F cm^{-2}.

3. Results and Discussion

3.1. EIS Investigation. Figure 1 shows the EIS plots in Nyquist format recorded from the MMI monolayer modified silver electrode and the blank in deaerated 0.5 M KCl and 2.5 mM $[Fe(CN)_6]^{3-}$/$[Fe(CN)_6]^{4-}$ solution. In Figure 1b, the high frequency region has a distinct Nyquist semicircle which is due to the existence of inhibitor film, comparing to the blank one (Figure 1a), indicating that the silver electrode modified by MMI monolayers shows the change of the corrosion kinetics at the surface and efficiently improves the anticorrosive performance.

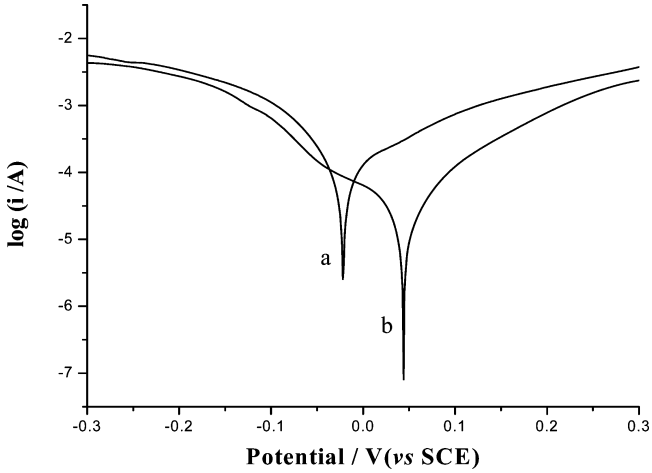

Figure 4. Tafel plot of a silver electrode in 0.5 M KCl and 2.5 mM $[Fe(CN)_6]^{3-}$/$[Fe(CN)_6]^{4-}$ solution: (a) blank and (b) with MMI monolayers, at a scan rate of 10 mV/s.

TABLE 3: Corrosion Potential, Corrosion Current Density, and Inhibition Efficiency, in 0.5 M KCl and 2.5 mM $[Fe(CN)_6]^{3-}$/$[Fe(CN)_6]^{4-}$ Solution for a Blank Silver Electrode and MMI Monolayers on the Silver Electrode

	E_{corr}/mV	I_{corr}/(mA·cm^{-2})	η/%
a. blank	−22	0.2076	
b. with MMI monolayers	44	0.03618	82.6

Depending upon the shape of the EIS spectrum, an equivalent circuit model is assumed and output by the ZsimpWin software. To obtain the fitting parameters, the program must fit the best frequency response of the given EIS spectrum, and the quality of the fitting is judged by how well the fitting curve overlaps the original spectrum. The curve fitting of EIS results for blank silver electrode and the MMI-modified silver electrode are shown in Figures 2 and 3, together with the equivalent circuits of *LR(QR)* and *LR(QR)(QR)* mode as the inset. The systems in

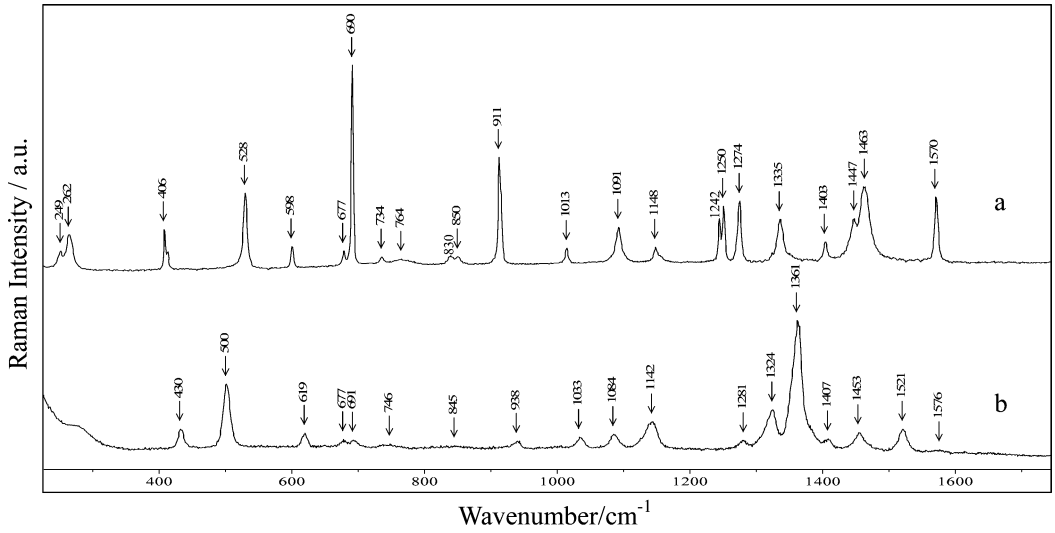

Figure 5. Normal Raman spectrum of solid MMI (a) SERS spectrum of MMI monolayers on the silver electrode (b).

TABLE 4: Assignment of Raman Spectra of Solid MMI and SERS B3LYP/LANL2DZ Calculated Vibrations of Its Thiol and Thione Forms[a] by Referring to the Literature[6]

solid (cm^{-1})	SERS (cm^{-1})	calculated —SH	calculated =S	approximate assignment
249w				$C^1{=}S^6$str.
262m		230		$N^2{-}C^7$ op.bend; $H^{10}{-}S^6$ op.bend
406m			393	ring rot.; $N^2{-}C^1{-}S^6$ bend; $N^5{-}C^1{-}S^6$ bend
	430m	411		ring rot.; $N^2{-}C^1{-}S^6$ bend; $N^5{-}C^1{-}S^6$ bend
528s	500s		501	$N^2{-}C^1{-}S^6$ bend; $N^5{-}C^1{-}S^6$ bend
598m	619m	614	625	ring op bend; ring CH op bend
677w	677w	670	659	ring op bend; ring CH (NH) op bend
690vs	691w	659	666	$C^1{-}N^2{-}C^7$ bend;$C^3{-}N^2{-}C^7$ bend
734vw	748vw	734	709	ring CH op bend
764vw				
830vw	845vw		839	ring CH op bend
850vw		868		$C^1{-}S^6{-}H$ ip. bend
	891m	891	895	ring bend; ring CH (NH) bend; $H{-}C^1{-}S^6$ bend
911s	922vw		911	ring bend; ring CH (NH) bend; $H{-}C^1{-}S^6$ bend
	938m	940	911	ring bend; ring CH(NH) bend; $C^1{-}S^6{-}H$ bend
1013w	1038m	1016		ring bend; ring CH bend; CHMe bend; $C^1{-}S^6{-}H$ bend
1091m	1084m	1069	1073	ring CN str.; ring CH(NH) bend
1148w	1142w	1133	1131	$C^1{=}S^6$ str.; ring CH bend
1242m				
1250s	1281m	1264	1256	ring breathing; $C^7{-}N^2$ str.; ring CH(NH) bend
1274s	1324s		1301	ring CN str.; ring bend; ring CH (NH) bend
1335m	1361vs	1360		ring CN str.; ring bend; ring CH bend
1403w	1407w	1402		ring CN str., $N^2{-}C^7$ str.; ring CH bend
1447m			1414	$C^1{=}S^6$ str.; ring CN str.; ring NH bend
1463s	1453m		1426	$C^1{=}S^6$ str.; ring CN str.; ring NH bend
	1521m	1511		$C^3{-}C^4$ str.; $C^6{-}N^1$ str.; ring CH bend
1570s	1576w		1565	$C^3{-}C^4$ str.; ring CH(NH) bend

[a] Abbreviations used: s, strong; m, medium; w, weak; br, broad; bend, bending; str., stretching; ip, in-plane; op, out-of-plane; Me, methyl.

which the solid/liquid interface was modeled by the simple equivalent circuit involved the parameters L, R_b, R_f, R_t, Q_f, and Q_d. L is the inductance. R_b represents the solution resistance between the working and reference electrodes. R_t expresses the charge transfer resistance whose amplitude reflects the capability of the electrode against corrosion reaction. Q_d shows the constant phase element (CPE) that was used to modify the double-layer capacitance of the C_d of the electrode for the purpose of obtaining more accurate fitting results. The n of Q_d ranging from 0.6 to 0.9 accounts for the CPE character of the capacitance. The MMI monolayer modified silver electrode is suited with the equivalent circuit mode of *LR(QR)(QR)*. The EIS parameters of the blank and MMI modified silver surface were listed in Tables 1 and 2, respectively. It should be mentioned that many noises from the instrumental sources lead to errors of EIS measurement because of the set frequencies covering several decades. Thus, the chi-square could be taken to give the relative error to weight the assumption between the simulated and experimental data. An acceptable agreement of the chi-square value is nearly 1×10^{-3}, and in the present fitting, it is about 7×10^{-3}.

Comparing to the blank silver electrode, the Q_f and R_f are a novel observation in the mode of the MMI coating silver surface. A capacitor Q_f (3.816×10^{-8} F/cm^2) corresponds to the MMI film capacity, because the coating is nonconductive to the electrode. A resistor R_f (8.248×10^4 Ω cm^2) indicates the conductive paths through the coating pores. As a result, it suggests that the MMI monolayers were successfully self-

SCHEME 2: Proposed Desorption Procedure for MMI from the Silver Surface with the Applied Potentials

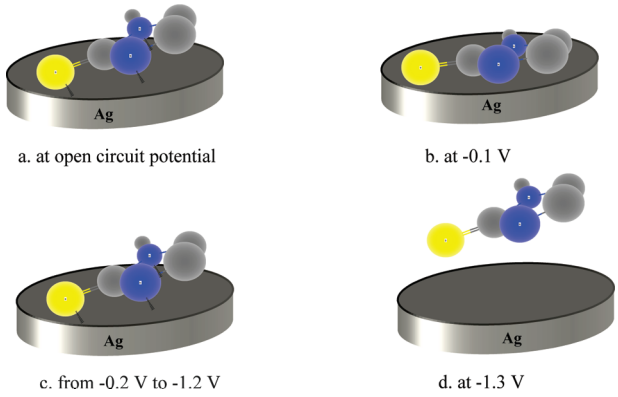

assembled onto the silver electrode and the film displayed an efficient anticorrosive behavior.

3.2. Studies of Electrochemical Polarization. In Figure 4, the electrochemical polarization curves of the silver electrodes without and with MMI monolayers are obtained in 0.5 M KCl and 2.5 mM $[Fe(CN)_6]^{3-}/[Fe(CN)_6]^{4-}$ solution at 25 °C. And the dynamic parameters of the corrosion potential (E_{corr}) and the corrosion current (I_{corr}) along with the inhibition efficiency,[32] η, are tabulated in Table 3.

The η is defined by $1 - I_{corr}(2)/I_{corr}(1)$, where $I_{corr}(1)$ and $I_{corr}(2)$ refer to corrosion current densities in the absence and presence of the MMI monolayers at the silver surface, respectively. From Table 3, it can be found that the corrosion potential of the silver electrode modified with MMI monolayers is of 44 mV, positively shifting by 66 mV in comparison to that of the blank silver electrode at −22 mV. The η of the modified silver electrode reaches nearly 82.6%. It proves that the silver electrode with MMI monolayers presents the high efficient anticorrosive capability. Its high efficient anticorrosive property should be contributed to the strong interaction between the MMI molecule and the surface. Therefore, the further SERS observations on the adsorption structure of the MMI monolayers were performed.

3.3. Raman Study. ***3.3.1. Normal Raman and SERS Spectroscopy.*** Figure 5 shows the normal Raman spectrum of the MMI in solid form and the SERS spectrum for the silver electrode with the MMI monolayers. The successful formation of MMI monolayers is confirmed with Raman observations conducted at 10 random points of the modified surface (Figure S1, Supporting Information). In Figure 5a, the prominent bands are observed at 1570, 1463, 1447, 1335, 1274, 1250, 1091, 911, 690, 528, and 406 cm^{-1}. On the basis of the B3LYP/LANL2DZ calculation results for MMI vibration reported by Biswas[6] et al. (given in Table 4), the 1570 and 1463 cm^{-1} peaks are assigned to the $C^3—C^4$ stretching and $C^1═S^6$ stretching. The peaks at 1447, 1335, and 1274 cm^{-1} are contributed to the ring CN stretch with contributions from ring bending and ring CH bending vibrations. The 1091 and 911 cm^{-1} bands are attributed to in-plane ring breathing and ring bending modes. The Raman bands at 690, 528, and 406 cm^{-1} are all pointed to the mixture of $C^1—N^2—C^7$ bending and $N^5—C^1—S^6$ bending. Two medium intensity bands are observed at 1250 and 406 cm^{-1}, which are assigned to ring breathing, ring CN stretch, and ring rotation, respectively. Thus, in the normal Raman spectrum, it indicates that the thione form of MMI in the solid state is preferential existence. However, the thiol form also cannot be completely excluded.

From Figure 5b, it could be found that all of the prominent peaks at 430, 500, 619, 691, 845, 938, 1033, 1084, 1142, 1281,1324, 1361, 1453, and 1576 cm^{-1} are from the thione form

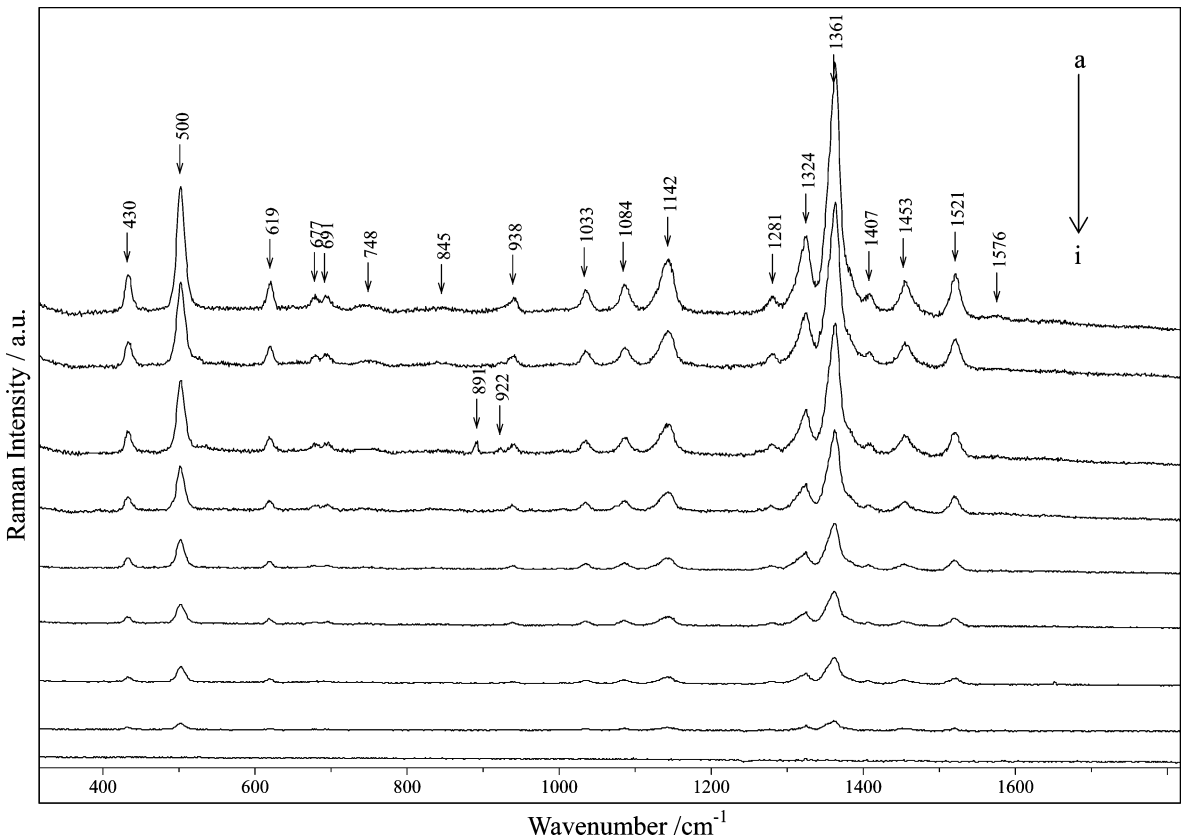

Figure 6. In situ SERS spectra of MMI at the Ag electrode surface in 0.1 M KCl solution: (a) open circuit potential, (b) −0.0, (c) −0.1, (d) −0.3, (e) −0.5, (f) −0.7, (g) −0.9, (h) −1.1, (i) −1.3 vs SCE.

of MMI. A strong peak at 500 cm^{-1} is assigned to cocontribution of $N^2—C^1—S^6$ bending and $N^5—C^1—S^6$ bending. The modes at 1324 and 1361 cm^{-1} are contributed to the ring CN stretch with contributions from ring bending and ring CH bending vibrations. The medium bands at 430, 619, 938, 1033, 1084, 1142, 1281, and 1453 cm^{-1} are attributed to the ring bending and breathing and ring CN stretching vibrations. The weak peaks at 691, 845, 1142, and 1576 cm^{-1} are assigned to the mixture of $C^1—N^2—C^7$ bending and $C^3—N^2—C^7$ bending, and the ring CH out-of-plane bending, and $C^1═S^6$ stretching, and the mixture of $C^1═S^6$ stretching, ring CN stretching, and ring NH bend, respectively. According to the SERS mechanism[33,34] and the surface selection rules,[35,36] the vibrational modes of groups that attach to or are very close to the surface should be more enhanced in the SERS spectrum and the vibrational modes with parallel polarizability components with respect to the surface will not be enhanced. Hence, the above-mentioned SERS bands are correlated with S^6, N^2, and N^5 atoms, indicating that they should be the direct adsorption sites and the azole ring is very close to the silver surface with a tilted orientation. A scheme of adsorption fashion of MMI monolayers at the silver surface is depicted in Scheme 2a.

3.3.2. In Situ SERS Electrochemical Investigation. To deepen comprehension of MMI monolayers, the in situ electrochemical SERS spectral experiments of the silver electrodes were conducted in 0.1 M KCl solution under applied potential from open circuit to −1.3 V vs SCE (shown in Figure 6). In Figure 6a, the spectral profile recorded at open circuit is the same as that of Figure 5b, illustrating that the MMI molecule at the silver surface kept the adsorption mode via the sites of the S^6, N^2, and N^5 atoms. When the potential was shifted to −0.1 V, two new bands at 891 and 922 cm^{-1} all from the mixture of ring bending, ring CH (NH) bending, and $H—C^1—S^6$ bending were enhanced. However, as the potential achieved at −0.2 V, the above-mentioned two peaks were disappeared. The extraordinary enhancement possibly resulted from the slight change of MMI adsorption fashion as the electrochemical hydrogen evolution reaction happened, during which the reaction intermediate with a matching energy level with the incident light was generated; thus, the effective charge transfer process could occur.[37] The intermediate state of adsorption fashion (the applied potential at −0.1 V) is that the azole ring further approaches the silver surface, resulting in a lying mode via S^6, N^2, and N^5 atoms. During the potentials from −0.2 to −1.2 V, the adsorption mode is also via the sites of the S^6, N^2, and N^5 atoms. The complete desorption of MMI from the interface of silver all happened when the potential was applied at −1.3 V vs SCE. The electrochemical desorption process is described in Scheme 2.

4. Conclusions

The relationship between the adsorption structure of MMI monolayers at the silver surface and its anticorrosion is studied by electrochemical and SERS techniques. By way of summary, the conclusions reached may be stated as follows:

(1) The EIS mechanism of the blank and the silver surface modified by MMI monolayers were fitted with the modes of *LR(QR)* and *LR(QR)(QR)*. The MMI monolayers on the silver surface presented a sound impedance behavior. Meanwhile, the Tafel plot also indicated that the MMI monolayers on the silver surface had a high anticorrosive efficiency (η around 82.6%).

(2) The formation of the monolayers at the silver surface is via the S^6, N^2, and N^5 atoms of the MMI molecule with a tilted orientation.

(3) On the basis of the in situ SERS observations of the electrochemical desorption process of MMI monolayers from the silver surface, existence of a medium adsorption state was found around the potential of the hydrogen evolution applied at about −0.1 V before its complete desorption.

Acknowledgment. This work was supported by the National Natural Science Foundation of China (Grant No. 20975068), Key Laboratory of Resource Chemistry of Ministry of Education, Leading Academic Discipline Project of Shanghai Normal University (Grant No. DZL706), the National Basic Research Program of China (Grant No. 2008CB617504), and the Foundation of Shanghai Normal University (Grant Nos. DYL200703 and DYL701).

Supporting Information Available: SERS spectra recorded from 10 random points at a silver electrode surface with MMI monolayers. This material is available free of charge via the Internet at http://pubs.acs.org.

References and Notes

(1) Merchant, B.; Lees, J. F.; Alexander, W. D. *Pharmacol. Ther., Part B* **1978**, *3*, 305.
(2) Weetman, A. P.; McGregor, A. M.; Hall, R. *Clin. Endocrinol.* **1984**, *21*, 163.
(3) Kendall-Taylor, P. *Br. Med. J.* **1984**, *288*, 509.
(4) Bentiss, F.; Traisnel, M.; Vezin, H.; Lagrenée, M. *Ind. Eng. Chem. Res.* **2000**, *39*, 3732.
(5) Subramanian, R.; lakshminarayanan, V. *Corros. Sci.* **2002**, *44*, 535.
(6) Biswas, N.; Thomas, S.; Sarkar, A.; Mukherjee, T.; Kapoor, S. *J. Phys. Chem. C* **2009**, *113*, 7091.
(7) Shriri, A.; Trachli, B.; Hajjaji, N.; Keddam, M.; Takenouti, H.; Frignani, A.; Zucchi, F. In 9th European Symposium on Corrosion Inhibitors. Ann. Univ.Ferrara, N.S., Sez:V, Suppl. N. 2000, *11*, 627.
(8) Kosec, T.; Milošev, I.; Pihlar, B. *Appl. Surf. Sci.* **2007**, *253*, 8863.
(9) Mamas, S.; Kiyak, T.; Kabasakaloglu, M.; Koc, A. *Mater. Chem. Phys.* **2005**, *93*, 41.
(10) Yang, H.; Sun, Y.; Ji, J.; Song, W.; Zhu, X.; Yao, Y.; Zhang, Z. *Corros. Sci.* **2008**, *50*, 3160.
(11) Sherif, E. S. M.; Erasmus, R. M.; Comins, J. D. *J. Colloid Interface Sci.* **2007**, *311*, 144.
(12) Yang, H.; Song, W.; Ji, J.; Zhu, X.; Sun, Y.; Yang, R.; Zhang, Z. *Appl. Surf. Sci.* **2008**, *255*, 2994.
(13) Otero, E.; Bastidas, J. M. *Werkst. Korros.* **1996**, *47*, 133.
(14) Zhang, R.; Yang, H.; Sun, Y.; Song, W.; Zhu, X.; Wang, N.; Wang, Y.; Pan, Y.; Zhang, Z. *J. Phys. Chem. C* **2009**, *113*, 9748.
(15) Sun, Y.; Song, W.; Zhu, X.; Zhang, R.; Pang, Q.; Zhang, Z.; Yang, H. *J. Raman Spectrosc.* **2009**, *40*, 1306.
(16) Contini, G.; Di Castro, V.; Angelaccio, A.; Motta, N.; Sgarlata, A. *Surf. Sci.* **2000**, *470*, L7.
(17) Di Castro, V.; Allegretti, F.; Baldacchini, C.; Betti, M. G.; Contini, G.; Corradini, V.; Lamastra, F.; Mariani, C. *Surf. Sci.* **2002**, *7*, 507.
(18) Mariani, C.; Allegretti, F.; Corradini, V.; Contini, G.; Di Castro, V.; Baldacchini, C.; Betti, M. G. *Phys. Rev. B* **2002**, *66*, 115407.
(19) Allegretti, F.; De Renzi, V.; Biagi, R.; Del Pennino, U.; Contini, G.; Di Castro, V.; Mariani, C.; Betti, M. G.; Fontanesi, C. *Surf. Sci.* **2003**, *539*, 63.
(20) Le Ru, E. C.; Blackie, E.; Meyer, M.; Etchegoin, P. G. *J. Phys. Chem. C* **2007**, *111*, 13794.
(21) Zhang, J.; Gao, Y.; Alvarez-Puebla, R. A.; Buriak, J. M.; Fenniri, H. *Adv. Mater.* **2006**, *18*, 3233.
(22) Michaels, A. M.; Jiang, J.; Brus, L. *J. Phys. Chem. B* **2000**, *104*, 11965.
(23) Kneipp, K.; Wang, Y.; Kneipp, H.; Perelman, L. T.; Itzkan, I.; Dasari, R. R.; Feld, M. S. *Phys. Rev. Lett.* **1997**, *78*, 1667.
(24) Nie, S.; Emory, S. R. *Science* **1997**, *275*, 1102.
(25) Talley, C. E.; Jackson, J. B.; Oubre, C.; Grady, N. K.; Hollars, C. W.; Lane, S. M.; Huser, T. R. *Nano Lett.* **2005**, *5*, 1569.
(26) Lal, S.; Grady, N. K.; Goodrich, G. P.; Halas, N. J. *Nano Lett.* **2006**, *6*, 2338.
(27) Jackson, J. B.; Halas, N. J. *Proc. Natl. Acad. Sci. U.S.A.* **2004**, *101*, 17930.
(28) Levin, C. S.; Bishnoi, S. W.; Grady, N. K.; Halas, N. *J. Anal. Chem.* **2006**, *78*, 3277.
(29) Shervedani, R. K.; HatefiMehrjardi, A. *Electrochim. Acta* **2007**, *52*, 7051.
(30) Zhou, A.; Xie, B.; Xie, N. *Corros. Sci.* **2000**, *42*, 469.

(31) Taniguchi, I.; Umekita, K.; Yasukouchi, K. *J. Electroanal. Chem.* **1986**, *202*, 315.

(32) Bockris, J.; Khan, S. *Surface Electrochemistry: A Molecular Level Approach*; Plenum Pub. Corp.: New York, 1993.

(33) Fe'lidj, N.; Aubard, J.; Le'vi, G.; Krenn, J. R.; Salerno, M.; Schider, G.; Lamprecht, B.; Leitner, A.; Aussenegg, F. R. *Phys. Rev. B* **2002**, *65*, 5419.

(34) McFarland, A. D.; Young, M. A.; Dieringer, J. A.; Duyne, R. V. *J. Phys. Chem. B* **2005**, *109*, 11279.

(35) Moskovits, M. *J. Chem. Phys.* **1982**, *77*, 4408.

(36) Moskovits, M.; Suh, J. S. *J. Phys. Chem.* **1984**, *88*, 5526.

(37) Liu, F.; Han, Q.; Chen, Y.; Zhong, Q.; Ren, B.; Tian, Z. *Electrochemistry* **2001**, *1*, 74.

JP911024D